Lab on a Chip

Accepted Manuscript

ROYAL SOCIETY OF CHEMISTRY

www.rsc.org/loc

Journal Name

Plug and Measure - a chip-to-world interface for photonic lab-on-a-chip applications[†]

Tobias Nils Ackermann,[*‡] Pablo Giménez-Gómez,[*] Xavier Muñoz-Berbel[*] and Andreu Llobera[*]

The integration of detection mechanisms with microfluidics may be one of the most promising routes towards widespread application of Lab-on-a-Chip (LoC) devices. Photonic detection methods like in the so-called Photonic Lab-on-a-Chip (PhLoC) have the advantage to be non-invasive, easy to sterilize and highly sensitive even with short integration times and thus allow in-situ monitoring and quantification of biological and chemical processes. The readout of such detection methods usually requires special training of potential users, as in most cases they are confronted with the need of establishing fiber-optics connections to and from the PhLoC and/or rely on the use of complex laboratory equipment. Here we present a low-cost and robust chip-to-world interface (CWI), fabricated by CO_2-laser machining, facilitating the non-expert use of PhLoCs. Fiber-optics with standard SMA-connectors (non-pigtailed) and PhLoCs can be plugged into the CWI without the need for further adjustments. This standardization bestows great versatility on the interface, providing a direct link between PhLoCs and a wide range of light sources and photo-detectors. The ease of use of the proposed simple plug mechanism represents a step forward in terms of user-friendliness and may approach PhLoC devices to practical applications.

1 Introduction

The field of microfluidics and Lab-on-a-Chip (LoC) has been envisioned to have tremendous potential to produce high throughput analytical tools pushing into pharmaceutical and biotech research[1,2] as well as practical devices for point-of-care (PoC) diagnostics, performing complex laboratory procedures on a microchip. A variety of microfluidic platforms have been developed in the last decade to control liquid movement on-chip[3] through components like micro-pumps[4,5], -valves[6] and -mixers[7–9]. Also, different detection schemes such as electrochemical[10] or optical measurements[11–13] in microfluidics have been validated in proof-of-concept studies, showing their potential advantages over laboratory tests[3,14,15]. Still, only a small percentage of published research based on LoCs and microfluidics has reached the stage of an actual implementation as a technology that enables biologists in their everyday research[16] or achieved successful introduction into the market as consumer products[17,18].

The main obstacle regarding a practical, user-friendly implementation of LoCs with any detection scheme remains in the development of robust connections from the device to the outside world (hereafter named 'interface'), allowing effective handling also by non-experts.[19,20] Regarding fluidic handling, a variety of robust connectors have been reported during the last decade[19,21–23]. Companies like *microfluidic ChipShop*, *Cellix* or *Dolomite*[24] offer entire series of already functionalised LoCs with fluidic connectors directly attached and compatible with their respective pumping systems. Most of the current commercialization models are directed towards a business-to-business (B2B) strategy involving the research and academic market instead of the development of a real end-user product.[25] Developers are now moving away from the idea of the single 'killer app' and are instead focusing their efforts on bridging the divide between industry and academia in the hopes of using microfluidics as an enabling technology for a wide range of life-science applications.[24] As one of the pursued development paths towards enhancing functionality, the integration of optical/optoelectronic elements with microfluidics has resulted in a new generation of highly sensitive and robust bio-sensors.[12,13,15] Optical detection schemes have the advantage to be non-invasive, easy to sterilize and potentially highly sensitive even with short integration times. This makes them particularly useful for monitoring of biological processes in applications like bio-assays and on-site monitoring in

* *Institut de microelectrónica (IMB-CNM), Campus UAB, E-08193 Cerdanyola del Vallès, Spain. Fax:(+34) 93 580 1496; Tel:(+34) 93 594 7700*
† Electronic Supplementary Information (ESI) available: [details of any supplementary information available should be included here]. See DOI: 10.1039/b000000x/
‡ corresponding Author; Tel:(+34) 93 594 7700 (ext. 2431); E-mail: tobias.ackermann@imb-cnm.csic.es

environmental studies but also for PoC diagnostics, where an immediate result is desired by the end-user.

While active components like photo-diodes promise fully incorporated detection and readout, such integration with the microfluidic platform is technologically challenging and expensive and in most examples [26–30] either light-source or detection remains 'off-chip' [11] or needs external stimuli (e.g. pumping lasers) for the integrated units to work.

Alternatively, the integration of passive photonic elements with microfluidics, as in the so-called Photonic Lab-on-a-Chip (PhLoC) [31], offer greatly simplified fabrication processes, as photonic and fluidic components can be defined in the same step and using low cost materials and processes. They would therefore be more suitable for PoC applications in the role of disposable cartridges. On the downside, potential users are confronted with the need to use external bulk optics and establish optical (and probably fluidic) connections to and from the PhLoC. Since microfluidic devices are often only used a few times, − typically only one to avoid cross contamination −, it would be desirable to easily insert (or replace) them in a holder (the 'interface'), where the fluidic, optical and maybe even electrical connections are made without any active alignment by the user. [12] Yet, for photonic applications to our knowledge no such interface has been presented to the scientific community to date.

In this work, we focus on this open issue and present a robust chip-to-world interface (CWI) fabricated and assembled by low-cost methods to facilitate fiber-optics coupling to PhLoCs for non-expert users. After introducing the involved design schemes and fabrication methodology, we compare the performance of the low-cost fiber-coupler to a commercial counterpart and present an experimental study exploring robustness and required alignment margins of the fully assembled CWI.

2 Design and working prinicple

Fig. 1a shows an emulator of a PhLoC only comprising a bent dielectric waveguide (WG) on a transparent substrate, which will serve us as a model for proof-of-concept. As illustrated, effective coupling to and from the WG occurs at specific relative coordinates and incident angles of 90° to the respective edges of the PhLoC.

The proposed chip-to-world interface (CWI) for such PhLoCs is depicted in Fig. 1b-d. The required precise relative positioning of fiber-optics connections and PhLoC is achieved by splitting the design-scheme in several independent building blocks. That way every unit can be fabricated separately in-plane, which makes it possible to take advantage of the full lateral resolution of the planar technologies used in this work. As shown in Fig. 1b, a robust outer frame composed of four interlocked blocks confines the PhLoC in the *y*-axis. To facilitate the insertion and removal of the PhLoC, an additional movable block is used to confine the space in *x*-direction and push the PhLoC in position after insertion - aligned with the fiber-optics (More information on the concrete building block design used in this work can be found in Fig. S1 and S3, ESI†). Figs. 1b-c depict the design-schemes of the blocks for the input (*y-z*) and output (*x-z*) plane respectively. A thin platform is anchored here at the required height level (*z*-position)
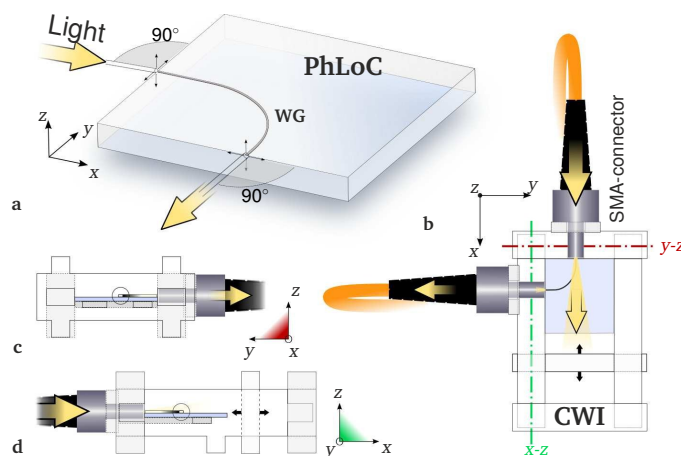

Fig. 1 Schematic illustration of chip-to-world interface concept.

to align the end-facets of the WG with the center of the circular opening representing the fiber-connector. The fiber-connections are optimized to facilitate plugging in and out of industrial standard SMA-connectors in order to increase the versatility and ease of use of the interface. As those connectors have standardized dimensions, the user can choose between a variety of fiber diameters without changing the design. A detailed model of the proposed fiber-connections (hereafter called 'plug-optics') can be found in Fig. S1, ESI.†

The design of the CWI and the photonic structures on the PhLoC respectively is coupled and based on the idea of trading coupling losses for a high signal-to-noise ratio. Concretely, we introduce the 90°bends in the WGs to achieve an optical output perpendicular to the optical input. In that way, independently of the in-coupling efficiency, the output will result from the light coupled into the photonic structure of the PhLoC (signal), while the non-confined light (noise) should not reach the readout. This approach allows us to use integrated photonic structures with far smaller dimensions than those of the input fiber-optics without spoiling the signal-to-noise ratio. Thus, the required alignment precision can be met by low-cost (and high throughput) fabrication while maintaining full functionality.

3 Materials and Methods

3.1 Materials

SU-8 2005 was purchased from *MicroChem Corp* and used as received. 4" borosilicate wafers were purchased from *SCHOTT AG* with a thickness of 0.7 mm. PMMA plates were purchased from *Ferreteria Maranges S.A* in thicknesses of 1 mm, 3 mm, and 5 mm and flexible polyurethane foam was purchased from *RS Components Ltd*.

3.2 PhLoC fabrication

For the fabrication of the dielectric waveguides, a 6 μm thick SU-8 layer was spincoated at 3000 rpm on O_2-plasma activated borosilicate (Pyrex®) wafers. The 90 μm wide waveguides (bend radius = 4 mm) were then defined via direct photolithography (see ESI† for details), resulting in a WG cross-section of $(90 \times 6)\,\mu m^2$. The wafer was cut using a diamond blade cutting

machine (safety distance $\equiv 25\,\mu m$ from the WG facets) to release the individual PhLoCs.

3.3 CO$_2$ laser processing

The CWI building blocks were fabricated via CO$_2$ laser processing of poly-methylmethacrylate (PMMA), which combines the attributes low-cost and minimum time consumption (being a one step process). Thus it is an ideal method for rapid prototyping as well as industrial level fabrication of the final product.

PMMA, while being highly transparent in the visible spectrum, acts as an excellent absorber in the far infrared and can therefore be very effectively processed by a CO$_2$ laser. In addition, its low weight together with reasonable hardness and low cost are perfect characteristics for a cheap and robust CWI.

In this work we used a commercially available Epilog Mini 24 laser writer employing a CO$_2$-laser (see Table 1 for specifications) for the fabrication. It can be directly addressed by a computer as one would a conventional printer. 2D-patterns designed as vector graphics are sent to the machine together with the desired configurations of power (P), writing speed (S) and laser pulse frequency (F). The combination of the latter parameters controls the gaussian beam shape of the laser and thus the line-width as a function of the penetration depth as described elsewhere[32].

For the fabrication of the CWI building blocks 1 mm, 3 mm, and 5 mm thick PMMA sheets were employed. With increasing thickness of the PMMA, the variation of the line-width as a function of depth becomes more important, resulting in a measurable difference between the line-width d_{top} at the top and d_{bottom} at the bottom of the PMMA sheet respectively. Thus, cutting conditions have been optimized for the 3 mm and 5 mm thick PMMA sheets with the aim to minimize this variation (compare Fig. S4, ESI†) and achieve vertical walls. We found that due to different mechanisms for the motion-control in x- and z-axis of the laser writer, the average line-width $\bar{d} = (d_{\text{top}} + d_{\text{bottom}})/2$ also differs depending on the direction of the cut.

Table 1 Characteristics of Epilog Mini 24.

working wavelength	10.62 μm
maximum power	24 W
maximum cutting speed	88.9 mm/s
resolution	1200 dpi max.
precision of xy-positioning	±12.7 μm

Table 2 Cutting conditions and corresponding line-widths for PMMA as used in the fabrication of the CWI elements. F is the laser pulse frequency in Hz, P the percentage of maximum power and S the percentage of maximum speed. The full characterization can be found in the supplementary material.†

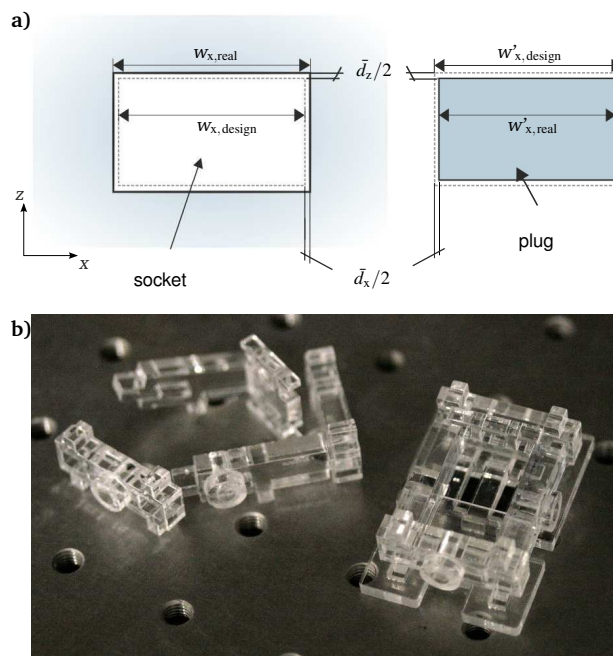| PMMA thickness	Conditions	Resulting average line-width $\bar{d}$
5 mm	$F = 5000$ $P = 100$ $S = 5$	$\bar{d}_x = 160\,\mu m \pm 30\,\mu m$ $\bar{d}_y = 220\,\mu m \pm 25\,\mu m$
3 mm	$F = 5000$ $P = 100$ $S = 7$	$\bar{d}_x = 235\,\mu m \pm 20\,\mu m$ $\bar{d}_y = 195\,\mu m \pm 10\,\mu m$

Fig. 2 a) Schematic illustration of the design schemes for the laser cutting of plugs and sockets and **b)** photograph of the laser fabricated constituent parts and the fully assembled CWI.

3.3.1 CWI assembly

The crucial part for robust interlocks between adjoining building blocks are the corresponding plugs and sockets. The relative dimensions were empirically optimized under consideration of the previous characterization of direction-dependent line-width as shown in Fig. 2a. For the best fitting of adjoining parts, a tolerance value of 150 μm was added to the desired dimension in x or y respectively according to $w_{\text{design}} = w_{\text{real}} \pm \bar{d} + 150\,\mu m$, where w_{real} is the desired dimension after fabrication and w_{design} the respective length introduced in the design scheme. The sign of $\bar{d}$ is positive when designing outer structures (plugs) and negative for inner structures (sockets). Some examples of fabricated individual building blocks and a completely assembled CWI are shown in Fig 2b.

3.4 Optical characterization

In all experiments, a fiber-coupled red laser (635 nm, 2.5 mW, Thorlabs, Inc.) connected to a FC/PC-SMA multimode fiber (Thorlabs, Inc.) with core/cladding diameter of 200/230 μm and numerical aperture NA of 0.22 was employed as light source. A QE Pro 65000 photo-spectrometer (Ocean Optics) served as detector. To obtain a 2D-mapping of the output plane, a pig-tailed 50/125 μm fiber was mounted on a motorized xz-stage (Micos VT80, Eschenbach, Germany) perpendicular to the edge of the PhLoC to scan the area around the WG end-facet with a step size of 10 μm. Movement and intensity acquisition were controlled by a LabVIEW script to obtain the complete mapping of the optical output plane (compare Fig. S5, ESI†). The intensity at 635 nm was collected at each point for constant input power of 0.25 mW and with an integration time of 25 ms. SMA-SMA mul-

timode fiber-optics (Thorlabs, Inc.) with core/cladding diameters of 50/125 µm, 105/125 µm and 200/230 µm and numerical aperture *NA* of 0.22 were used to evaluate the plug-optics individually and in their function as chip-to-world interface.

3.5 Simulations

Ray-tracing simulations emulating the experimental conditions were performed using TracePro (Lambda Research) for comparison. To that effect $8 \cdot 10^5$ rays with a wavelength of 635 nm were traced through a 3D-model of the PhLoC from a perfectly aligned, 2 m long input fiber-optics with *NA* of 0.22. The waveguide's modal profile was examined in form of the irradiance map on the output plane at 200 µm distance from the edge of the PhLoC.

4 Results and discussion

4.1 Evaluation of plug-optics

In order to assess the reproducibility and performance of the proposed plug-optics connectors, three sets of plug-optics were fabricated and assembled in all possible combinations to form a three-slot fiber-to-fiber connector. To that end, they were interlocked with and held together by auxiliary bottom- and top-pieces (detailed schemes can be found in the ESI†, Fig. S2). Fiber-to-fiber coupling was evaluated by averaging the coupled intensity over the three combinations and the resulting plug-optics triplets. For constant input intensity, the average output intensity was recorded as a function of the size of the output fiber-optics. The results compared to a commercial two-slot fiber-connector are presented in Fig. 3. The statistical evaluation shows that there are no significant differences between coupled intensities obtained using either of the connectors. The plug-optics connectors though show more variation as a result of low-cost fabrication and assembly. This variation becomes more important, the more similar the diameters of input and output fiber-optics.
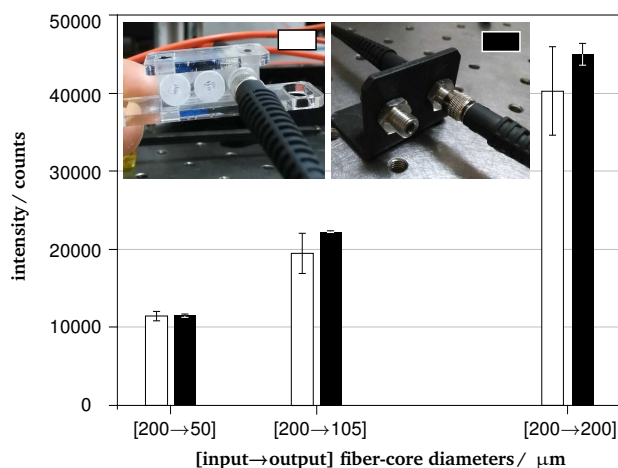

Fig. 3 Evaluation of the 'plug optics' concept. Average intensities coupled from fiber-optics to fiber-optics using plug-optics and a two-slot commercial fiber-connector are compared.

4.2 Plug and Measure

From the evaluation of the plug-optics coupler it would seem that size mismatch between emitting and receiving end ensures reliable and reproducible, if inefficient coupling. Robust fiber-to-chip coupling should therefore be viable using the proposed CWI in the case of sufficient size mismatch between on-chip photonics and fiber-optics. As another consequence, an important fraction of the incoming light would not be coupled to the WG, but propagate as stray light through the structure and may thus to some extent contribute as noise to the optical readout.

4.2.1 Signal-to-Noise Ratio (SNR)

In this context, as a next step we assessed the contribution of stray light to the output signal on the basis of the previously described PhLoC. An intensity mapping of the output plane in an area *A* of (500×500) µm² around the center of the WG and at a distance of 200 µm from the edge of the PhLoC was used to assess the Signal-to-Noise Ratio (SNR). Simulated and experimental results are presented in Fig. 4.

Fig. 4a shows the light propagation through the model PhLoC according to the ray-tracing simulation conducted with TracePro. Due to inefficient coupling (insertion losses of 15.4 dB are to be expected according to the simulation), a large portion of incoming rays result in stray light. Yet, no stray light reaches the output plane: The irradiance map obtained from the rays incident on *A* shows no measurable incident radiation apart from a localized and sharply peaked intensity profile corresponding to the multi-modal SU-8 waveguide with (90×6) µm² cross-section. As a result of the high numerical aperture of the WG, an extensive
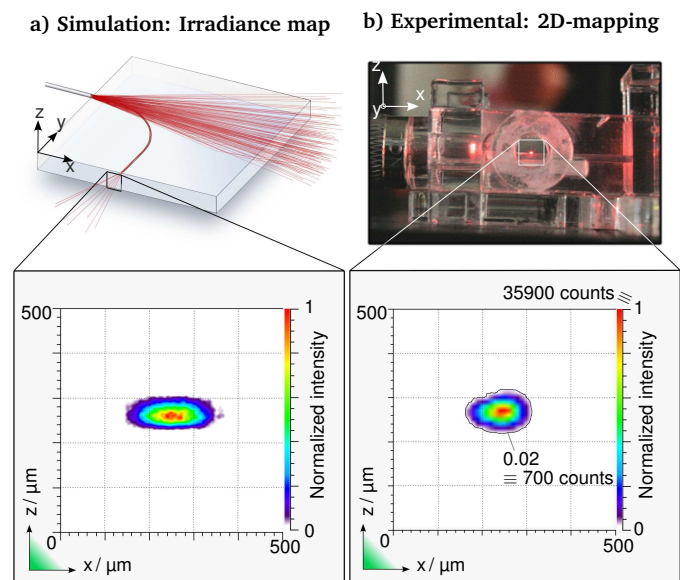

a) Simulation: Irradiance map   **b) Experimental: 2D-mapping**

Fig. 4 a) Ray-tracing simulation (using TracePro, Lambda Research) of a 90° bent SU-8 waveguide (cross-section (6×90) µm²) on glass substrate. $8 \cdot 10^5$ rays with a wavelength of 635 nm are traced through the model via a 2 m long fiber-optics (200/230 µm, $NA = 0.22$) aligned with the waveguide. An irradiance map shows the intensity profile of the waveguide output on the x-z plane at 200 µm distance from the waveguides end-facet. **b)** (500×500) µm² 2D-mapping around the WG output obtained by pig-tailed 50/125 µm fiber-optics mounted on a motorized stage and the resulting 3D-profile.

expansion of this profile with the distance from the end-facet of the waveguide could be expected. This is reflected in the profile's dimensions of roughly $200\,\mu m$ in x-direction and $70\,\mu m$ in z-direction found in the irradiance map.

Fig. 4b shows the experimental fiber-to-chip coupling using the proposed CWI and 2D-mapping of the resulting output profile. In the photograph, the end facet of the WG can be identified as a confined bright spot in the center of the small square, which corresponds to the scanning area A. The picture demonstrates that light is coupled successfully via the plug-optics to the thin SU-8 waveguide and guided through the bend to the output. The mapping result shows a localized and sharply peaked region of high intensity (signal S) with a maximum peak intensity of $S_{\max} = 35900\,\text{counts} \equiv 1$ corresponding to the WG output. It is worth noting that the experimental output profile is more localized than the simulated one. This can be attributed to the low numerical aperture of the scanning fiber-optics. While in the simulation all rays incident on A contribute to the profile, radiation at large angles is discarded in the experiment. The contour line in the 2D-profile marks the threshold between what can be considered waveguide output and background noise N and defines profile with effective width of $\approx 160\,\mu m$ in x-dimension. In the scanned area outside the contour line, the recollected intensity does not exceed a maximum of $N_{\max} = 700\,\text{counts} \equiv 0.02$. We therefore assume that as a consequence of the introduced WG bend, stray-light indeed does not contribute as noise to the readout on the output plane. Hence, in the case of optimal alignment of the receiving $50/125\,\mu m$ fiber-optics with the waveguide output and relatively low input power of $0.25\,mW$, we achieve a signal-to-noise ratio of $\mathrm{SNR} = S_{\max}/N_{\max} = 50$.

The sharpness of the intensity profile indicates that, depending on the diameter of the fiber-optics employed as output, small deviations in alignment and positioning may result in significant variations of the readout. On the other hand, in sight of the measured SNR fiber-optics with large (up to $500\,\mu m$) core diameters could be used for the readout in order to provide sufficient alignment margins and achieve maximum output without significant noise contribution. In the following, we explore the robustness and repeatability of the readout provided by the proposed CWI applying different alignment margins.

4.2.2 Robustness and repeatability of measurements

The completely assembled CWI, with PhLoC as well as fiber-optics input and output plugged in, is shown in Fig. 5a. In this configuration we studied the influence of fabrication precision, assembly/disassembly and repeated positioning and alignment of PhLoC and fiber-optics on the output signal. The input unit (compare Fig. 1c) was fabricated twice and, exchanging this part between each measurement and plugging the PhLoC in anew, the output intensity was collected subsequently by different output fiber-optics. Varying the diameter of the output fiber-optics results in different overlap situations of fiber-optics and the intensity profile originating from the WG. As apparent from Fig. 5a, misalignment may produce strong variations of signal intensity using a $50/125\,\mu m$ fiber as output, while using a $200/230\,\mu m$ fiber the intensity may well be invariable to small misalignments.
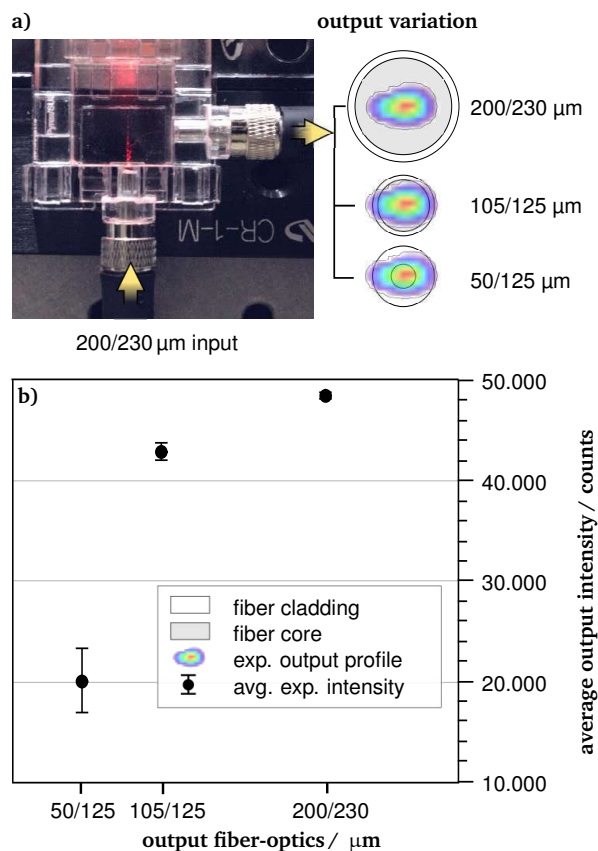

Fig. 5 a Plug and measure. Photograph of CWI with plugged PhLoC and fiber-optics showing fiber-connection and light coupling to and from the PhLoC. For different output fiber-optics, the relative dimensions of the experimental output intensity profile at $200\,\mu m$ distance from the WG and the fiber-optics cross-sections are shown schematically. **b** Measured intensities corresponding to different fiber-optics configurations. The error bars correspond to experimental intensity variations of $7.5\,\%$ using $50/125\,\mu m$, $3.3\,\%$ using $105/125\,\mu m$ and $0.6\,\%$ using $200/230\,\mu m$ fiber-optics as output respectively.

As shown in Fig. 5b, the experimental value obtained by the $50/125\,\mu m$ fiber-optics indeed shows significant variation. Using $105/125\,\mu m$ fiber-optics this variation is greatly reduced and using the $200/230\,\mu m$ fiber-optics, no significant signal variation was obtained.

These results are in line with the previous findings and show that the combined alignment variations induced by fabrication precision (compare Table 1), repeated assembly/disassembly and plugging in and out of the PhLoC are fully compensated by the alignment margins of $\pm 20\,\mu m$ provided by using $200/230\,\mu m$ fiber-optics for input and output.

Together with the obtained $\mathrm{SNR} = 50$, this validates the proposed methodology of fabrication and assembly as a robust and cheap solution for PhLoC-to-world connections which could be employed beneficially in a series of already developed PhLoCs with different approaches integrating for instance optical spectroscopy[31,33], flow cytometry[34–38] or photonic whispering gallery mode (WGM) structures for label-free molecular detection[39,40] in microfluidic systems.

5 Conclusions

We have presented a cheap, robust and easy-to-use chip-to-world interface for photonic lab-on-a-chip devices (PhLoCs). Comparing the proposed plug-optics SMA fiber-connections by themselves to a commercial fiber-to-fiber connector, we found that the performance was not significantly different. This standardization gives great versatility to the interface, providing a direct link between PhLoCs and a wide range of light sources and photo-detectors. Experimental evaluation of the fully assembled CWI showed that the introduction of bends in the photonic structure allowed to efficiently discard stray-light artefacts and obtain a clean signal with good signal-to-noise ratio (SNR = 50). In this optimized configuration it could be shown that alignment margins of ± 20 suffice to fully compensate misalignments induced by fabrication or assembly. Even through different cycles of fabrication and assembly as well as plugging in and out of the PhLoC, coupling to SU-8 multimode waveguides as thin as 6 μm has been demonstrated without significant signal variation.

The fact that PhLoCs can be easily plugged in and out by a user without a special skill-set while obtaining full functionality is a big step forward in terms of user-friendliness and potentially brings PhLoCs one step closer towards practical applications.

6 Acknowledgements

References

1 D. J. Beebe, G. A. Mensing and G. M. Walker, *Annual review of biomedical engineering*, 2002, **4**, 261–286.

2 C. Haber, *Lab on a chip*, 2006, **6**, 1118–1121.

3 D. Mark, S. Haeberle, G. Roth, F. von Stetten and R. Zengerle, *Chemical Society reviews*, 2010, **39**, 1153–82.

4 D. J. Laser and J. G. Santiago, *Journal of Micromechanics and Microengineering*, 2004, **14**, R35–R64.

5 P. Woias, *Sensors and Actuators, B: Chemical*, 2005, **105**, 28–38.

6 K. W. Oh and C. H. Ahn, *Journal of Micromechanics and Microengineering*, 2006, **16**, R13–R39.

7 V. Hessel, H. Löwe and F. Schönfeld, *Chemical Engineering Science*, 2005, **60**, 2479–2501.

8 N.-T. Nguyen and Z. Wu, *Journal of Micromechanics and Microengineering*, 2005, **15**, R1–R16.

9 C. Y. Lee, C. L. Chang, Y. N. Wang and L. M. Fu, *International Journal of Molecular Sciences*, 2011, **12**, 3263–3287.

10 D. G. Rackus, M. H. Shamsi and A. R. Wheeler, *Chemical Society Reviews*, 2015, **44**, 5320–5340.

11 B. Kuswandi, Nuriman, J. Huskens and W. Verboom, *Analytica Chimica Acta*, 2007, **601**, 141–155.

12 K. B. Mogensen and J. P. Kutter, *Electrophoresis*, 2009, **30**, 92–100.

13 M. C. Estevez, M. Alvarez and L. M. Lechuga, *Laser & Photonics Reviews*, 2012, **6**, 463–487.

14 G. M. Whitesides, *Nature*, 2006, **442**, 368–373.

15 N. Pires, T. Dong, U. Hanke and N. Hoivik, *Sensors*, 2014, **14**, 15458–15479.

16 E. K. Sackmann, A. L. Fulton and D. J. Beebe, *Nature*, 2014, **507**, 181–9.

17 C. D. Chin, V. Linder and S. K. Sia, *Lab on a Chip*, 2012, **12**, 2118.

18 L. R. Volpatti and A. K. Yetisen, *Trends in Biotechnology*, 2014, **32**, 347–350.

19 C. K. Fredrickson and Z. H. Fan, *Lab on a chip*, 2004, **4**, 526–533.

20 M. I. Mohammed, S. Haswell and I. Gibson, *Procedia Technology*, 2015, **20**, 54–59.

21 E. Wilhelm, C. Neumann, T. Duttenhofer, L. Pires and B. E. Rapp, *Lab on a chip*, 2013, **13**, 4343–51.

22 D. van Swaay, J.-P. Mächler, C. Stanley and A. DeMello, *Lab on a chip*, 2014, **14**, 178–81.

23 Y. Temiz, R. D. Lovchik, G. V. Kaigala and E. Delamarche, *Microelectronic Engineering*, 2015, **132**, 156–175.

24 N. Blow, *Nature Methods*, 2007, **4**, 665–670.

25 H. Becker, *Lab on a chip*, 2009, **9**, 2119–2122.

26 R. Horvath, H. C. Pedersen, N. Skivesen, C. Svanberg and N. B. Larsen, *Journal of Micromechanics and Microengineering*, 2005, **15**, 1260–1264.

27 S. Balslev, A. M. Jorgensen, B. Bilenberg, K. B. Mogensen, D. Snakenborg, O. Geschke, J. P. Kutter and A. Kristensen, *Lab on a chip*, 2006, **6**, 213–217.

28 X. Wang, M. Amatatongchai, D. Nacapricha, O. Hofmann, J. C. de Mello, D. D. C. Bradley and A. J. de Mello, *Sensors and Actuators, B: Chemical*, 2009, **140**, 643–648.

29 A. Llobera, J. Juvert, A. González-Fernández, B. Ibarlucea, E. Carregal-Romero, S. Büttgenbach and C. Fernández-Sánchez, *Light: Science & Applications*, 2015, **4**, e271.

30 G. de Cesare, A. Nascetti, R. Scipinotti, A. Zahra and D. Caputo, *Sensing and Bio-Sensing Research*, 2015, **3**, 53–58.

31 I. Rodríguez-Ruiz, T. N. Ackermann, X. Muñoz-Berbel and A. Llobera, *Analytical Chemistry*, 2016.

32 S. Prakash and S. Kumar, *International Journal of Precision Engineering and Manufacturing*, 2015, **16**, 361–366.

33 A. Prabhakar and S. Mukherji, *International Conference on Systems in Medicine and Biology, ICSMB 2010 - Proceedings*, 2010, 67–70.

34 B. R. Watts, Z. Zhang, C.-Q. Xu, X. Cao and M. Lin, *Biomed.Opt.Express*, 2012, **3**, 2784–2793.

35 P. Fei, Z. Chen, Y. Men, A. Li, Y. Shen and Y. Huang, *Lab on a Chip*, 2012, **12**, 3700–3706.

36 J. Godin, C. H. Chen, S. H. Cho, W. Qiao, F. Tsai and Y. H. Lo, *Journal of Biophotonics*, 2008, **1**, 355–376.

37 J. Godin, V. Lien and Y. H. Lo, *Applied Physics Letters*, 2006, **89**, 2006–2008.

38 Z. Wang, J. El-Ali, M. Engelund, T. Gotsaed, I. R. Perch-Nielsen, K. B. Mogensen, D. Snakenborg, J. P. Kutter and A. Wolff, *Lab on a Chip*, 2004, **4**, 372–377.

39 T. Wienhold, S. Kraemmer, A. Bacher, H. Kalt, C. Koos, S. Koe-ber and T. Mappes, *Optics Express*, 2015, **23**, 1025.

40 U. Bog, F. Brinkmann, S. F. Wondimu, T. Wienhold, S. Kraemmer, C. Koos, H. Kalt, M. Hirtz, H. Fuchs, S. Koeber and T. Mappes, *Advanced Science*, 2015, 1–6.

Graphical abstract
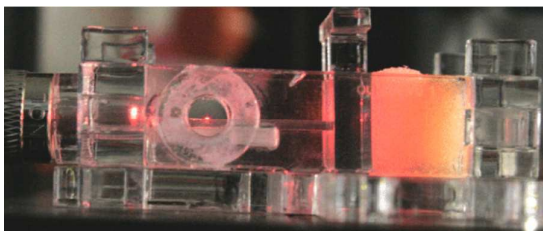
Robust and reusable chip-to-world interface fabricated and assembled by low-cost methods to facilitate standard SMA-connector fiber-coupling to photonic lab-on-a-chips.